SoftwareX 36 (2026) 103030

Contents lists available at ScienceDirect

SoftwareX

journal homepage: www.elsevier.com/locate/softx

Original Software Publication

An interactive online platform for the simulation and analysis of LIBS

Yilin Wang [a,*], Shuo Zhang [a], Toni Aaltonen [a], Pekka Suominen [b], Eetu Ojanen [a]

[a] RoboAI Research Centre, Satakunta University of Applied Sciences, Pori, Finland
[b] School of Technology and Innovation, University of Vaasa, Wolffintie 32, Vaasa, 65200, Finland

ARTICLE INFO

Keywords:
Libs
Spectrum
Plasma emission simulation
Time-resolved spectroscopy

ABSTRACT

Physics-based OES/LIBS simulation tools range from locally installed packages to lightweight web calculators, but few currently combine browser-based zero-installation access with full configurability over multi-layer plasma structure, inter-layer temperature and density gradients, time-resolved plasma evolution, and instrumental resolution — the combination needed for realistic synthetic dataset generation and method development. We present a hosted service layer that exposes SAMK's (Satakunta University of Applied Sciences) in-house LTE-based OES/LIBS spectrum simulator as a free community resource. The contribution is not a new simulation model; rather, it focuses on making a previously developed simulator easy to access, configure, and run in both interactive and programmatic workflows.

The service includes (1) a browser-based application with interactive visualisation and (2) a pip-installable Python package providing a stable API for automated parameter sweeps and bulk requests. Users can define elemental composition, set electron temperature (Te) and electron density (Ne), and configure plasma decay parameters. The interface supports multi-layer plasma descriptions, allowing users to specify the number of layers, their spatial dimensions, and Te/Ne ratios between layers to approximate plasma inhomogeneities. Instrumental resolution settings can also be adjusted to generate realistic simulated device outputs. Results are retrievable as CSV for quick inspection or HDF5 for large-scale structured datasets, with full metadata to ensure reproducibility.

Metadata

Nr	Code metadata description	*Metadata*
C1	Current code version	v1.0
C2	Permanent link to code/ repository used for this code version	Python client repository: https://github.com/RoboAI-Green/roboai-libs-client Web frontend repository: https://github.com/RoboAI-Green/roboai-libs-ui
C3	Permanent link to reproducible capsule	
C4	Legal code license	MIT License.
C5	Code versioning system used	Git
C6	Software code languages, tools and services used	Python, JavaScript, React, FastAPI
C7	Compilation requirements, operating environments and dependencies	Python 3.11+, Node.js 18+
C8	If available, link to developer documentation/manual	
C9	Support email for questions	yilin.wang@samk.fi, shuo.1.zhang@samk.fi, toni.aaltonen@samk.fi, eetu.ojanen@live.com, pekka.suominen@uwasa.fi

1. Motivation and significance

Laser-Induced Breakdown Spectroscopy (LIBS) is a widely used analytical technique that generates characteristic atomic emission spectra from laser-ablated plasma, enabling rapid elemental identification in fields ranging from industrial quality control and materials characterisation to environmental monitoring and space exploration [1–4]. Physics-based simulation of LIBS spectra under the Local Thermodynamic Equilibrium (LTE) approximation is a well-established approach for spectral interpretation, parameter optimisation, and the generation of synthetic training datasets for machine learning models

* Corresponding author.
E-mail addresses: yilin.wang@samk.fi (Y. Wang), shuo.1.zhang@samk.fi (S. Zhang), toni.aaltonen@samk.fi (T. Aaltonen), pekka.suominen@samk.fi (P. Suominen), eetu.ojanen@live.com (E. Ojanen).

https://doi.org/10.1016/j.softx.2026.103030
Received 6 July 2026; Received in revised form 27 August 2026; Accepted 10 September 2026
Available online 15 September 2026

[5–8].

Although some browser-based LIBS simulators exist, such as the NIST LIBS Database, they typically offer limited configurability — lacking support for multi-layer plasma modelling, inter-layer gradient control, time-resolved dynamics, or programmatic batch access [9]. Beyond existing web tools, researchers requiring full configurability must typically implement the simulation physics independently, a barrier that disproportionately affects groups without dedicated computational expertise.

The software presented here addresses this gap by exposing an in-house LTE LIBS simulator as a freely accessible hosted service. The contribution is not a new simulation model; rather, it provides a service layer that removes installation barriers and delivers two complementary interfaces: (1) an interactive browser-based application, and (2) a pip-installable Python client library that enables scripted access for automated workflows. This design allows both experimentalists who prefer graphical interaction and computational researchers who require batch access to benefit from the same underlying physics engine. Spectral line data, derived from the NIST Atomic Spectra Database [10], are hosted server-side, requiring users only to access the web interface or install the lightweight Python client package.

2. Software description

This software provides a web-based platform for simulating LIBS emission spectra under LTE conditions. It supports static and time-resolved plasma simulations, multi-layer self-absorption modelling, and data export in multiple formats, accessible via a browser interface, FastAPI, or Python client library.

2.1. Software architecture

The system follows a client–server architecture built around a server-side simulation engine. The engine is exposed through a FastAPI backend and can be accessed by two user-facing clients: an interactive React web frontend and a lightweight Python client library.

2.1.1. Simulation engine

The scientific calculation engine is executed server-side and is accessed through the service interfaces provided by this work. Spectral line and level data from the NIST Atomic Spectra Database [10] are stored in a local server-side database. For each simulation, the engine retrieves the relevant transitions for the requested elements and resolves the plasma composition under the LTE assumption using partition functions, the Saha equation, and Boltzmann level populations [11,12]. Line emission and absorption coefficients are then evaluated on the selected wavelength grid, including Doppler, natural, and approximate Stark broadening estimates. For multi-layer plasma configurations, each line-of-sight layer is assigned its own temperature and electron density, and the emergent spectrum is obtained by combining layer emission and absorption through optical-depth attenuation.

2.1.2. Backend (FastAPI)

The backend service exposes the simulator through API endpoints. It receives simulation requests from the web frontend or Python client, validates input parameters, invokes the simulation engine, and returns structured JSON responses or downloadable export files. The backend also handles element-list queries, static spectrum calculations, dynamic time-resolved simulations, and HDF5 export generation.

2.1.3. Frontend (React + vite)

The browser interface (https://libs.roboai.fi) is a single-page application built with React and Vite. It communicates with the backend exclusively through the REST API and requires no local Python environment. The full frontend source code is available in this repository; users wishing to customise or extend the interface can follow the local development instructions in the repository README to install dependencies and run a local development server.

2.1.4. Python client library

The Python client library provides a programmatic interface to the hosted simulator for scripts, notebooks, and automated workflows. It is designed as a lightweight pip-installable package that wraps the backend service calls with Python functions, so users do not need to manually construct HTTP requests or interact with the internal calculation engine. Users can specify elements, molar proportions, wavelength sampling, plasma parameters, instrumental broadening, and export options using standard Python objects.

The client returns structured simulation results, including wavelength arrays, intensity arrays, spectral-line metadata, and, for dynamic simulations, time-dependent plasma parameters and time–wavelength intensity matrices. This enables batch parameter sweeps and synthetic spectrum generation for downstream analysis or machine-learning model training. The client library does not contain the internal simulation engine or the atomic database; all numerical calculations are performed by the backend service.

2.2. Software functionalities

2.2.1. LTE spectrum generation

The simulator generates wavelength-resolved LIBS emission spectra under the assumption of local thermodynamic equilibrium (LTE). Users specify one or more atomic species, their molar fractions x_a, the electron temperature T_e, and the electron number density N_e. The calculation may be performed on either a uniformly sampled wavelength interval or a user-supplied wavelength grid.

Atomic transition probabilities, level energies, and statistical weights are obtained from a local database derived from the NIST Atomic Spectra Database [10]. For each element a, the fractional populations $f_{a,z}$ of the ionization stages z are calculated from the Saha equilibrium [11]. The mean charge of the element is

$$\bar{z}_a = \sum_z z f_{a,z}.$$

The total heavy-particle number density N_{tot} is determined by enforcing charge neutrality for the complete mixture:

$$N_{\mathrm{e}} = N_{\mathrm{tot}} \sum_a x_a \bar{z}_a.$$

Consequently,

$$N_{\mathrm{tot}} = \frac{N_{\mathrm{e}}}{\sum_a x_a \bar{z}_a}, \qquad N_{a,z} = x_a N_{\mathrm{tot}} f_{a,z},$$

where $N_{a,z}$ is the number density of ionization stage z of element a. Within each ionization stage, level populations are calculated using the Boltzmann distribution:

$$N_{a,z,i} = N_{a,z} \frac{g_i}{U_{a,z}(T_{\mathrm{e}})} \exp\left(-\frac{E_i}{k_{\mathrm{B}} T_{\mathrm{e}}} \right),$$

where E_i and g_i are the level energy and statistical weight, and $U_{a,z}$ is the partition function.

For a transition from upper level u to lower level l, the wavelength-dependent emission and net absorption coefficients are evaluated as

$$\varepsilon_{\lambda,ul} = \frac{hc}{4\pi\lambda_{ul}} A_{ul} N_u \phi_{ul}(\lambda),$$

and

$$\kappa_{\lambda,ul} = \frac{\lambda_{ul}^4}{8\pi c} A_{ul} \left(\frac{g_u}{g_l} N_l - N_u \right) \phi_{ul}(\lambda),$$

respectively [13]. The negative $\boldsymbol{N_u}$ term accounts for stimulated emission. The total coefficients in each plasma layer are obtained by summing over all contributing transitions and elements:

$$\varepsilon_\lambda = \sum_{\mathrm{ul}} \varepsilon_{\lambda,\mathrm{ul}}, \qquad \kappa_\lambda = \sum_{\mathrm{ul}} \kappa_{\lambda,\mathrm{ul}}.$$

The intrinsic line profile $\phi_{ul}(\lambda)$ is represented by a pseudo-Voigt profile [14,15]. Its Gaussian component accounts for thermal Doppler broadening, while its Lorentzian component combines natural and electron-impact Stark broadening. Rather than sampling the profile only at the centre of each output bin, the profile area intersecting each wavelength bin is evaluated and divided by the bin width. This reduces sampling artefacts when the intrinsic linewidth is narrower than the wavelength-grid spacing. After radiative transfer has been evaluated, optional instrumental broadening is applied to the emergent spectrum by convolution with either a Gaussian or Lorentzian kernel of user-defined FWHM. Instrumental broadening is therefore treated separately from the intrinsic plasma line profile.

2.2.2. Time-resolved simulation

The dynamic mode uses empirical, user-adjustable parameterizations for the temporal evolution of the plasma. The exact functions used in the software are empirical implementation choices, not equations directly taken from the cited studies. In the present implementation, the user-defined reference values are normalized at a chosen reference time:

$$\mathrm{T_e(t)} = \frac{\alpha_\mathrm{T}}{(1+\beta_\mathrm{T}\mathrm{t})^{\gamma_\mathrm{T}}}, \mathrm{N_e(t)} = \frac{\alpha_\mathrm{N}}{(1+\beta_\mathrm{N}\mathrm{t})^{\gamma_\mathrm{N}}}.$$

where $\boldsymbol{t}$ is expressed in ns. The constants $(\boldsymbol{\alpha_T})$ and $(\boldsymbol{\alpha_N})$ are chosen so that $(\boldsymbol{T_e}(\boldsymbol{t_{\mathrm{ref},T}}))$ and $(\boldsymbol{N_e}(\boldsymbol{t_{\mathrm{ref},N}}))$ match the user-defined reference temperature and density. By default, both reference times are 100 ns.

The line-of-sight plasma length is represented by a simplified exponential saturation model,

$$L(t) = L_{\max}\left[1 - \exp\left(-\frac{t}{\tau}\right)\right],$$

which provides a compact approximation of plume expansion for exploratory simulation. Because the temporal evolution of electron temperature, electron density, and plume length depends strongly on experimental geometry, background gas, laser conditions, and detection timing, all decay and expansion parameters are exposed to the user and should be adjusted or refitted for a specific experiment. The default values are fitted internally to representative time-resolved copper LIBS data [16] and are intended as starting values rather than universal constants.

All snapshots in a time series are computed under the LTE assumption of Section 2.2.1. This assumption is least justified at the earliest times, when the plasma is still ionizing, and at the latest times, when the electron density has fallen; users should verify that the conditions of interest are compatible with LTE and should treat instantaneous spectra at the extremes of the time range as indicative rather than quantitative (Section 2.3).

2.2.3. Layered radiative transfer and self-absorption

The line-of-sight plasma column is represented by $\boldsymbol{H}$ plane-parallel homogeneous layers ordered from the plasma core ($\ell = \mathbf{0}$) to the observer-facing boundary ($\ell = \boldsymbol{H} - \mathbf{1}$). Within each layer, $\boldsymbol{T_{\mathrm{e},\ell}}, \boldsymbol{N_{\mathrm{e},\ell}}$, the geometrical path length $\boldsymbol{L_\ell}$, and the resulting emission and absorption coefficients are assumed to be spatially constant.

In the uniform mode, the plasma is represented by one homogeneous layer. This mode still includes finite-optical-depth attenuation within the layer, but it contains no spatial temperature or density gradient. The weak-gradient and strong-gradient presets use two layers consisting of a core and an outer layer. For both temperature and electron density, the outer-to-core ratios are 0.95 in the weak-gradient preset and 0.70 in the strong-gradient preset. In the custom mode, the number of layers and the temperature and density ratios may be specified by the user. For scalar ratios $\boldsymbol{r_T}$ and $\boldsymbol{r_N}$, the layer parameters are

$$\boldsymbol{T_{\mathrm{e},\ell}} = \boldsymbol{T_{\mathrm{e},0}}\boldsymbol{r_T^{\ell}}, \qquad \boldsymbol{N_{\mathrm{e},\ell}} = \boldsymbol{N_{\mathrm{e},0}}\boldsymbol{r_N^{\ell}}.$$

The user may additionally specify the total line-of-sight length and the fraction assigned to the core layer; the remaining length is distributed equally among the outer layers.

Scattering is neglected, and radiation propagation along the line of sight is described by

$$\frac{\mathbf{d}\boldsymbol{I_\lambda}}{\mathbf{d}\boldsymbol{s}} = \boldsymbol{\varepsilon_\lambda} - \boldsymbol{\kappa_\lambda}\boldsymbol{I_\lambda}, \qquad \boldsymbol{S_\lambda} = \frac{\boldsymbol{\varepsilon_\lambda}}{\boldsymbol{\kappa_\lambda}},$$

where $\boldsymbol{S_\lambda}$ is the source function. The optical depth of layer ℓ is

$$\boldsymbol{\tau_{\lambda,\ell}} = \boldsymbol{\kappa_{\lambda,\ell}}\boldsymbol{L_\ell}.$$

Because the coefficients are constant within each layer, the formal solution is evaluated analytically [13]. Assuming zero incident radiation at the rear boundary, the emergent intensity is

$$\boldsymbol{I_\lambda^{\mathrm{out}}} = \sum_{\ell=\mathbf{0}}^{\boldsymbol{H}-1} \boldsymbol{S_{\lambda,\ell}}\left[1 - \exp\left(-\boldsymbol{\tau_{\lambda,\ell}}\right)\right] \exp\left(-\sum_{\boldsymbol{m}=\ell+\mathbf{1}}^{\boldsymbol{H}-1} \boldsymbol{\tau_{\lambda,m}}\right).$$

The first factor represents radiation emitted by layer ℓ after absorption within that layer. The final exponential is the transmission through all layers located between layer ℓ and the observer. This formulation accounts for line-of-sight self-absorption and can produce line-centre self-reversal when radiation from a hotter core pass through a cooler, optically thick outer layer. This homogeneous-zone treatment of self-absorption follows established practice in LIBS modelling [17], in particular two-region descriptions of the laser-induced plasma that reproduce measured self-absorbed and self-reversed line profiles [18].

The implementation evaluates this expression vectorially over all wavelength bins and layers. Transfer within each layer is therefore treated using the analytical formal solution rather than finite-difference integration along the line of sight. The calculation assumes one-dimensional line-of-sight transport with no scattering or externally incident radiation.

2.2.4. Data export and reproducibility

Simulation results can be exported in several formats. CSV exports provide quick access to spectrum arrays and spectral-line tables for external plotting or spreadsheet inspection. HDF5 exports store structured numerical arrays, including wavelength grids, spectra, time-series data, and time–wavelength matrices for dynamic simulations. JSON responses are available through the API and are used by the web interface and Python client.

The web interface also supports saving and loading complete simulation configurations as JSON files. A saved configuration records the selected elements, proportions, wavelength sampling, plasma model, temporal parameters, and instrument-broadening settings. Together with a fixed software version and database version, these configuration files support reproducible reruns and parameter studies.

2.2.5. Programmatic access

Programmatic access is provided through the Python client described in Section 2.1.4, enabling scripted parameter sweeps and automated data generation.

2.3. Limitations and scope

The simulator assumes local thermodynamic equilibrium throughout and does not enforce a validity criterion as a precondition for running a simulation. The McWhirter criterion provides a first check on whether the selected conditions are compatible with LTE, and automatic reporting of this threshold in the simulation output metadata is planned

for a future release. It is, however, a necessary and not a sufficient condition for LTE in transient, spatially inhomogeneous laser-induced plasmas [19], since relaxation-time and diffusion criteria must also hold; a rigorous non-LTE treatment would require collisional-radiative modelling, for which complete rate data are unavailable for most elements.

Departures from LTE are largest at the earliest times, when the plasma is still ionizing, and at the latest times, as it cools and the electron density falls. In the latter case the emissivity decays faster still — the continuum scales as N_e^2 and line emissivity fall steeply through the Saha–Boltzmann factors — so the epochs in which LTE is weakest contribute least to a time-integrated spectrum. Instantaneous spectra at the extremes of the time range, and strongly self-absorbed resonance lines, for which the cool peripheral plasma dominates the absorption while contributing little emission, should therefore be interpreted with more caution.

The radiative transfer treatment is one-dimensional along the line of sight, and each layer is internally uniform, so continuous spatial gradients are represented only to the resolution of the chosen layer count. The model does not include scattering, frequency redistribution, externally incident radiation, multidimensional transport, or radiative feedback on the LTE level populations; full resonance-photon trapping and lateral transport are therefore outside its scope. Simulated line intensities and line ratios in the optically thick regime should accordingly be regarded as physically representative rather than quantitatively predictive, and quantitative use of strongly self-absorbed lines should be supported by experimental calibration.

3. Illustrative examples

3.1. Static spectrum simulation

As a first illustrative example, the software was used to generate the default static spectrum for nickel.

The resulting view shows the simulated emission spectrum together with line markers for the contributing transitions from the local NIST ASD-backed database (Figs. 1–3).

3.2. Time-resolved spectrum

The second example illustrates the dynamic simulation mode. The software produced both the full time-integrated exposure spectrum and spectra at individual time points selected with the time slider.

3.3. 3D visualization

This example focuses on the 3D wavelength–time–intensity surface generated from the dynamic simulation matrix. The surface view helps users inspect how emission features appear, decay, or persist across the simulated exposure window.

3.4. Programmatic access

For example, a static spectrum can be requested either from Python:

```
from roboai_libs_client import RoboAILIBSClient
  client = RoboAILIBSClient()
  result = client.simulate_static(elements=["Ni"], range_min_nm=280,
  range_max_nm=330)
```

The same simulation can also be launched from the command line for quick export.

```
roboai-libs static –element Ni –range 280 330 –out ni.csv
```

4. Impact

This software lowers the barrier to physics-based LIBS spectral simulation by reducing local installation requirements and providing

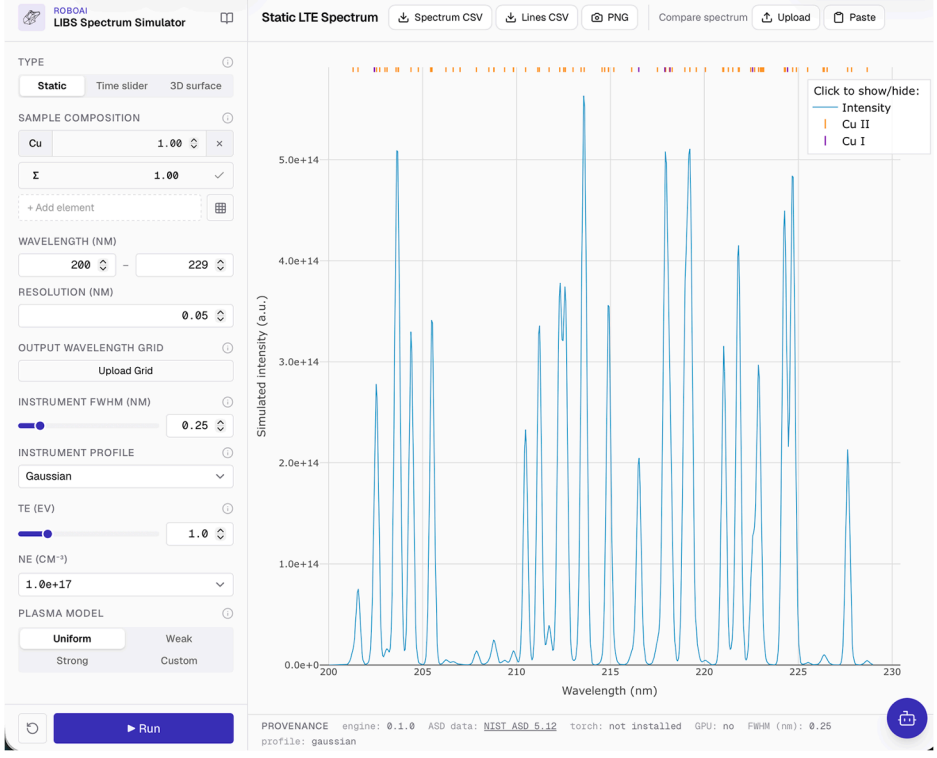

Fig. 1. Browser interface for static LTE spectrum simulation, showing nickel input parameters, spectral-line markers, and the simulated emission spectrum with CSV/HDF5 export options.

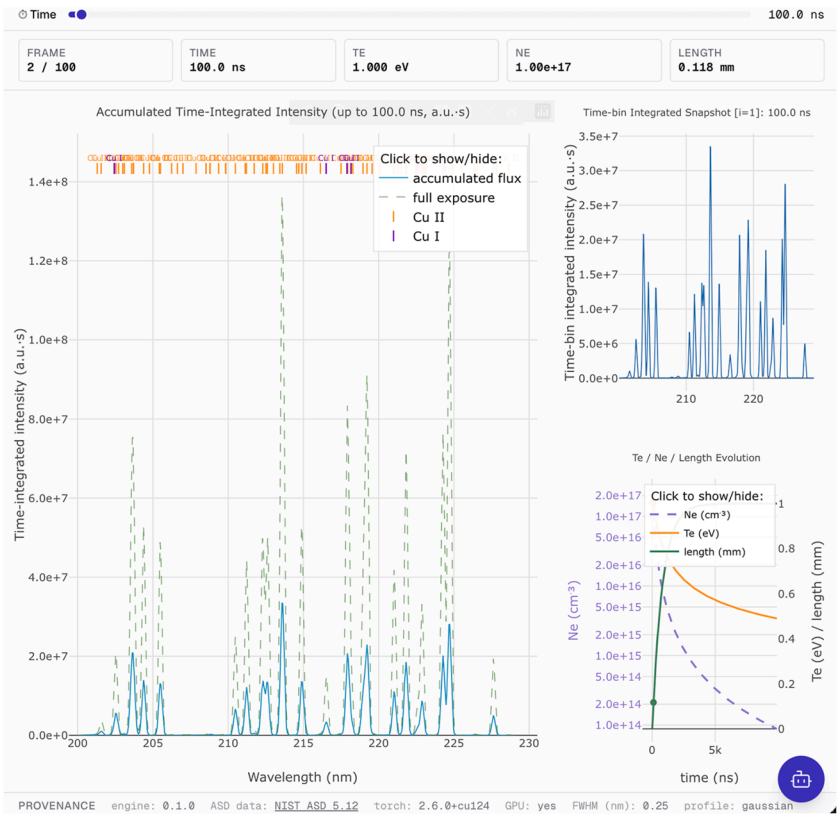

Fig. 2. Dynamic simulation view showing the time slider, accumulated and instantaneous spectra, plasma parameter evolution.

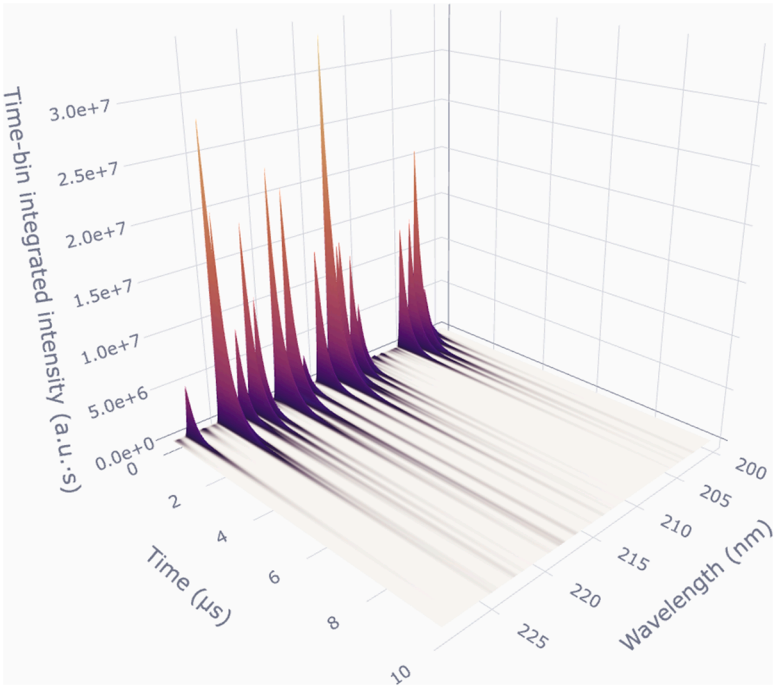

Fig. 3. Time-resolved 3D spectral surface showing the evolution of simulated emission intensity across wavelength and time.

both interactive and programmatic access modalities.

The primary beneficiaries are:

- Experimentalists who need a rapid qualitative reference for spectral line identification and interpretation of LIBS measurements without setting up a local simulation environment.
- Computational researchers and machine learning practitioners who require synthetic LIBS spectra for model development, sensitivity

studies, or benchmarking. The Python client enables automated parameter sweeps over electron temperature, electron density, elemental composition, instrumental broadening, and plasma configuration, while metadata-annotated HDF5 outputs support reproducible downstream analysis.
- Educators using LIBS or plasma spectroscopy in teaching contexts, where the web interface provides an accessible way to demonstrate how plasma parameters, elemental composition, and instrumental broadening affect emission spectra.

By exposing a previously internal simulator through user-facing web and Python interfaces, this work improves access to physics-based spectral simulation workflows. The programmatic access layer allows the simulator to be integrated into automated workflows and custom laboratory software and enables batch generation of synthetic spectra for machine-learning model training without requiring users to interact directly with the internal calculation engine.

5. Conclusions

This work presents a web-accessible service layer for LTE-based LIBS spectrum simulation, making a previously internal tool available through browser-based and programmatic interfaces with minimal local setup. The service provides an interactive web application and a lightweight Python client for scripted workflows. Key capabilities include static LTE spectra, time-resolved gate-integrated simulations with empirical plasma time-history models, configurable line-of-sight plasma layering for self-absorption studies, instrumental broadening, and CSV/HDF5 data export. Save/load configuration support further enables reproducible and shareable workflows.

The primary contribution is not a new physical model, but the reduction of the practical barrier between an established simulation engine and its potential users, including experimentalists performing spectral interpretation, computational researchers generating synthetic spectra, and educators demonstrating plasma-spectroscopy principles.

The original simulation engine used in this project was developed by Eetu Ojanen during his tenure at SAMK [16].

Declaration of generative AI and AI-assisted technologies in the manuscript preparation process

During the preparation of this work, the authors used Claude and ChatGPT/Codex, for manuscript translation, language refinement, and software-development support. The authors reviewed and edited the output as needed and take full responsibility for the content of the published article.

CRediT authorship contribution statement

Yilin Wang: Writing – original draft, Visualization, Software. **Shuo Zhang:** Writing – review & editing, Visualization, Software. **Toni Aaltonen:** Writing – review & editing, Software. **Pekka Suominen:** Writing – review & editing, Software. **Eetu Ojanen:** Methodology, Software.

Declaration of competing interest

The authors declare that they have no known competing financial interests or personal relationships that could have appeared to influence the work reported in this paper.

Acknowledgements

The work was carried out within the ROSS (Raskasmetallien online spektroskopia Satakunnassa) project at Satakunta University of Applied Sciences (SAMK), which aims to develop real-time online monitoring systems for heavy metal emissions in industrial processes using optical emission spectroscopy and AI-based analytics. The project is co-funded by the European Union Just Transition Fund (JTF) and SAMK.

References

[1] Anabitarte F, Cobo A, Lopez-Higuera JM. Laser-induced breakdown spectroscopy: fundamentals, applications, and challenges. ISRN Spectrosc 2012;2012:1–12. https://doi.org/10.5402/2012/285240.
[2] Noll R. Laser-induced breakdown spectroscopy: fundamentals and applications. Laser-Induc Breakdown Spectrosc: Fundam Appl 2012:1–543. https://doi.org/10.1007/978-3-642-20668-9.
[3] Wiens RC, Maurice S, Barraclough B, Saccoccio M, Barkley WC, Bell JF, Bender S, Bernardin J, Blaney D, Blank J, Bouyé M, Bridges N, Bultman N, Caïs P, Clanton RC, Clark B, Clegg S, Cousin A, Cremers D, Cros A, Deflores L, Delapp D, Dingler R, D'Uston C, Darby Dyar M, Elliott T, Enemark D, Fabre C, Flores M, Forni O, Gasnault O, Hale T, Hays C, Herkenhoff K, Kan E, Kirkland L, Kouach D, Landis D, Langevin Y, Lanza N, Larocca F, Lasue J, Latino J, Limonadi D, Lindensmith C, Little C, Mangold N, Manhes G, Mauchien P, McKay C, Miller E, Mooney J, Morris RV, Morrison L, Nelson T, Newsom H, Ollila A, Ott M, Pares L, Perez R, Poitrasson F, Provost C, Reiter JW, Roberts T, Romero F, Sautter V, Salazar S, Simmonds JJ, Stiglich R, Storms S, Striebig N, Thocaven JJ, Trujillo T, Ulibarri M, Vaniman D, Warner N, Waterbury R, Whitaker R, Witt J, Wong-Swanson B. The ChemCam instrument suite on the Mars Science Laboratory (MSL) rover: body unit and combined system tests. Space Sci Rev 2012;170:167–227. https://doi.org/10.1007/S11214-012-9902-4.
[4] Harmon RS, DeLucia FC, McManus CE, McMillan NJ, Jenkins TF, Walsh ME, Miziolek A. Laser-induced breakdown spectroscopy – An emerging chemical sensor technology for real-time field-portable, geochemical, mineralogical, and environmental applications. Appl Geochem 2006;21:730–47. https://doi.org/10.1016/J.APGEOCHEM.2006.02.003.
[5] Gąsior P, Gromelski W, Kastek M, Kwaśnik A. Analysis of hydrogen isotopes retention in thermonuclear reactors with LIBS supported by machine learning. Spectrochim Acta Part B At Spectrosc 2023;199:106576. https://doi.org/10.1016/J.SAB.2022.106576.
[6] Cristoforetti G, De Giacomo A, Dell'Aglio M, Legnaioli S, Tognoni E, Palleschi V, Omenetto N. Local thermodynamic equilibrium in laser-induced breakdown spectroscopy: beyond the McWhirter criterion. Spectrochim Acta Part B At Spectrosc 2010;65:86–95. https://doi.org/10.1016/J.SAB.2009.11.005.
[7] Favre A, Bultel A, Morel V, Lesage M, Gosse L. MERLIN, an adaptative LTE radiative transfer model for any mixture: validation on Eurofer97 in argon atmosphere. J Quant Spectrosc Radiat Transf 2025;330:109222. https://doi.org/10.1016/J.JQSRT.2024.109222.
[8] P.B. Hansen, Modeling of LIBS spectra obtained in martian atmospheric conditions, (2022). https://doi.org/10.18452/25303.
[9] NIST LIBS Database, (n.d.). https://physics.nist.gov/PhysRefData/ASD/LIBS/libs-form.html (accessed April 17, 2026).
[10] A R, Yu RJ, Kramida NAT. Atomic spectra database. NIST; 2024. https://doi.org/10.18434/T4W30F. |.
[11] Griem HR. Principles of plasma spectroscopy. Princ Plasma Spectrosc 1997. https://doi.org/10.1017/CBO9780511524578.
[12] Ciucci A, Corsi M, Palleschi V, Rastelli S, Salvetti A, Tognoni E. New procedure for quantitative elemental analysis by laser-induced plasma spectroscopy. Appl Spectrosc 1999;53:960–4. https://doi.org/10.1366/0003702991947612.
[13] Rybicki GB, Lightman AP. Radiative processes in astrophysics. Radiat Process Astrophys 1985. https://doi.org/10.1002/9783527618170.
[14] Thompson P, Cox DE, Hastings JB. Rietveld refinement of Debye–Scherrer synchrotron X-ray data from Al2O3. J Appl Crystallogr 1987;20:79–83. https://doi.org/10.1107/S0021889887087090.
[15] Olivero JJ, Longbothum RL. Empirical fits to the Voigt line width: a brief review. J Quant Spectrosc Radiat Transf 1977;17:233–6. https://doi.org/10.1016/0022-4073(77)90161-3.
[16] Ojanen E. Laser-induced plasma lifetime and emission spectrum modeling: generating simulated spectral data for neural network training. http://www.theseus.fi/handle/10024/914800; 2026 (accessed May 12, 2026).
[17] Bulajic D, Corsi M, Cristoforetti G, Legnaioli S, Palleschi V, Salvetti A, Tognoni E. A procedure for correcting self-absorption in calibration free-laser induced breakdown spectroscopy. Spectrochim Acta Part B At Spectrosc 2002;57:339–53. https://doi.org/10.1016/S0584-8547(01)00398-6.
[18] Aguilera JA, Bengoechea J, Aragón C. Curves of growth of spectral lines emitted by a laser-induced plasma: influence of the temporal evolution and spatial inhomogeneity of the plasma. Spectrochim Acta Part B At Spectrosc 2003;58:221–37. https://doi.org/10.1016/S0584-8547(02)00258-6.
[19] Cristoforetti G, De Giacomo A, Dell'Aglio M, Legnaioli S, Tognoni E, Palleschi V, Omenetto N. Local thermodynamic equilibrium in laser-induced breakdown spectroscopy: beyond the McWhirter criterion. Spectrochim Acta Part B At Spectrosc 2010;65:86–95. https://doi.org/10.1016/J.SAB.2009.11.005.